Published in *Canadian Journal of Civil Engineering* (In Press) **2019**

Use of mode shape ratios for pier scour monitoring in two-span integral bridges under changing environmental conditions

Malekjafarian, A.[a,1], Prendergast, L.J.[b,2,*], OBrien, E.[a,3]

[a] School of Civil Engineering,
University College Dublin,
Newstead,
Belfield,
Dublin 4,
Ireland

[b] Department of Civil Engineering,
Faculty of Engineering,
University of Nottingham,
Nottingham,
NG7 2RD,
United Kingdom

Email: [1]abdollah.malekjafarian@ucd.ie, [2]luke.prendergast@nottingham.ac.uk,
[3]eugene.obrien@ucd.ie

*Corresponding author

Abstract

In this paper, a novel pier scour indicator is introduced, which uses the ratio between mode shape amplitudes identified at two points on an integral bridge structure to monitor the progression of scour erosion. The Mode Shape Ratio (MSR) is investigated as an additional parameter to complement the use of changes in natural frequency as a scour indicator. The approach is demonstrated using numerical modelling and the MSR is extracted from acceleration signals arising in the structure due to modelled ambient and vehicle-induced vibrations. The MSR shows higher sensitivity to scour erosion than the more commonly researched natural frequency. Furthermore, the variation in MSR under temperature fluctuations is inversely related to that of frequency, in that it increases with increasing temperature whereas frequency decreases with increasing temperature. This inverse relationship potentially enables the separation of the scour effect from the temperature influence on the dynamics of the system.

Keywords: scour; temperature; bridge; mode shape, Frequency Domain Decomposition; SHM.

1. Introduction

The erosive action of water removing soil from around bridge foundations is termed scour (Hamill 1999) and poses a serious problem for many bridge structures. It is the primary cause of bridge failure worldwide (Shirole and Holt 1991, Melville and Coleman 2000, Briaud et al. 2001, Wardhana and Hadipriono 2003) and constitutes a significant cost burden for infrastructure managers between inspections, repairs and preventative measures (Prendergast and Gavin 2014). Following recent failures (Maddison 2012), scour monitoring is receiving increasing interest among asset owners. Traditionally, diving inspections were adopted (Avent and Alawady 2005); however these tend to be subjective, labor-intensive and dangerous to undertake during flooding, when the likelihood of scour occurrence is highest. Moreover, as scour holes tend to refill with sediment upon subsidence of floodwaters, this can pose challenges for the success of visual-based assessment procedures. Remote monitoring systems are under increasing development, and often require the installation or operation of a device close to a foundation element to ascertain the time-varying scour condition (De Falco and Mele 2002, Hunt 2009, Yu 2009, Briaud et al. 2011, Zarafshan et al. 2012, Fisher et al. 2013, Prendergast and Gavin 2014, Kong et al. 2017). These systems, while broadly effective at detecting scour depths with varying accuracy, often miss the critical effect that scour has on the structural stability and safety. In effect, these systems typically cannot ascertain the distress experienced by a structure due to the presence of a scour hole.

Recognizing that scour changes the static and dynamic behavior of bridges has given rise to the area of vibration-based bridge scour monitoring (Briaud et al. 2011, Foti and Sabia 2011, Prendergast et al. 2013, 2016a, Elsaid and Seracino 2014, Chen et al. 2014, Klinga and Alipour 2015, Fitzgerald et al. 2019b). Dynamically monitoring structures can provide an inference of

the system stiffnesses and this can indicate the presence (and sometimes extent) of scour. To date, a significant majority of studies have focused on the effect of scour on the natural frequencies of structures (Briaud et al. 2011, Chen et al. 2014, Klinga and Alipour 2015, Prendergast et al. 2016a, 2017, 2018, Bao et al. 2017). Some studies have investigated other dynamic parameters such as the ratio of root-mean-square accelerations in various directions (Briaud et al. 2011), the variance of accelerations along a foundation to detect asymmetric behavior (Foti and Sabia 2011), mode-shape curvature and flexibility-based deflections (Elsaid and Seracino 2014, Xiong et al. 2018), among other methods. One issue that is often neglected in previous studies is the influence of temperature on the performance of vibration-based scour monitoring approaches. Temperature fluctuations can alter the material properties, which affects the dynamic characteristics. Specifically, a change in bridge temperature alters the natural frequency (Sohn et al. 2004), and since most scour detection methods rely on an analysis of frequency changes, this can pose problems. This effect has been studied in other (non-scour related) damage-detection fields (Limongelli 2010). For example, Farrar *et al.* (1994) investigated the change in measured frequency of the I-40 bridge in New Mexico, USA, when one of the girders was gradually cut (to represent a propagating crack). Theoretically, the bridge frequency should decrease with increasing progression of the cut, since the cut reduces the stiffness of the beam. In reality, the bridge frequency was observed to increase for the first two damage levels. It was subsequently discovered that the ambient temperature of the bridge during the experiment governed the response characteristics, and over-shadowed the changes due to the damage.

In this paper, the use of a novel scour-sensitive indicator is investigated, namely the Mode Shape Ratio (MSR), as an additional variable to aid in circumventing temperature influences. The MSR is obtained as the ratio of mode shape amplitudes identified from acceleration signals

89 measured at two points on an integral bridge-type structure. Knowledge of bridge mode shapes
90 can be valuable in dynamic investigations (Malekjafarian and OBrien 2014, 2017) and can be
91 used for damage detection (Chang and Kim 2016, OBrien and Malekjafarian 2016). This study
92 develops on that presented in Prendergast et al. (2016a), which investigated if scour around the
93 central pier of a two-span integral bridge could be detected by analyzing changes in the
94 structure's first natural frequency when excited by a vehicle. This paper uses MSR, obtained
95 from Frequency Domain Decomposition (FDD) analysis (Brincker et al. 2001) on generated
96 acceleration data, to infer the presence of scour in a typical integral bridge - see Fig. 1. Since
97 the same information is used as that required to determine the frequency (i.e. acceleration
98 signals), no further instrumentation requirements arise from this method. MSR is potentially a
99 more scour-sensitive parameter than natural frequency alone, and when combined with
100 frequency, may be capable of assisting in the separation of temperature-induced effects from
101 the effects of scour. Section 2 presents the numerical modelling undertaken to test the approach.
102 Section 3 introduces the MSR concept. Section 4 presents an analysis of the effect of scour on
103 frequency and MSR measurements. Section 5 investigates the influence of a changing
104 temperature environment on the resulting frequency and MSR values. Finally, section 6
105 discusses the applicability of the approach to real structures.

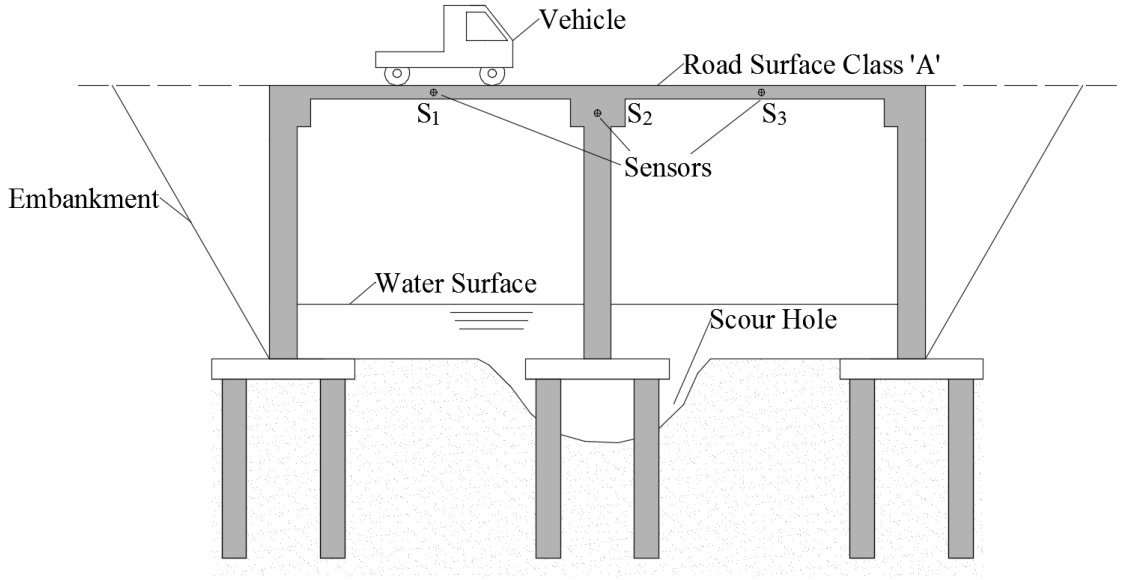

Fig. 1. System schematic with sensor layout, S1 – vertical mid-span acceleration, S2 – horizontal pier top acceleration and S3 – vertical mid-span acceleration

2. Numerical Modelling

The approach is investigated in this paper using numerical modelling, as it is impractical to perform large-scale bridge scour tests on real bridges. The model used in the present study is presented in detail in Prendergast et al. (2016b); however for clarity relevant details of the model are reproduced herein. The model consists of a two-span integral bridge founded on piles, which is loaded by both vehicular and ambient (environmental) loading. The vehicle model incorporates vehicle-bridge interaction effects, to make the responses as realistic as possible for the purpose of testing the MSR approach. The various modelling components are programmed in the MATLAB programming environment using a matrix formulation for the elements. The following sub-sections briefly present the bridge model (section 2.1), the soil-foundation model (section 2.2), scour modelling (section 2.3), and the loading (ambient and vehicle, section 2.4).

123 **2.1 Integral bridge model**

124 A two-span integral bridge model with flexible-support abutments, as presented in (Prendergast
125 et al. 2016b, 2017), is chosen to test the MSR technique. The reason for choosing an integral
126 bridge is deliberate as (i) the presence of moment connections between the supports and the
127 deck enables a mode shape ratio approach, as postulated in this paper, to be applied for scour
128 monitoring and (ii) integral construction is becoming more prevalent due to construction ease
129 and the lack of necessity for thermal expansion joints (O'Brien et al. 2015, Prendergast et al.
130 2016b). The properties of the two-span integral bridge model adopted in this paper are
131 presented in Table 1 (see Prendergast et al. (2016b) for detailed explanation of modelling
132 components).

133

134 Table 1. Integral bridge properties

Element	**Property**	**Value**
Bridge Deck Elements	EI (kN m^2)	0.1032×10^9
	ρA (kg m^{-1})	22.84×10^3
	Span length (m)	25
	Number of spans	2
LHS Abutment Elements	EI (kN m^2)	0.8694×10^6
	ρA (kg m^{-1})	4.241×10^3
	Abutment column length (m)	6
	Number of columns	9
Pier Elements	EI (kN m^2)	39 806 550
	ρA (kg m^{-1})	17 325
	Pier length (m)	6
	Number of piers (leaves)	2
RHS Abutment Elements	EI (kN m^2)	1.0626×10^6
	ρA (kg m^{-1})	4.241×10^3
	Abutment column length (m)	6
	Number of columns	9
Abutment Pile Elements	EI (kN m^2)	2.2266×10^6
	ρA (kg m^{-1})	6.7858×10^3
	Pile length (m)	15
	Number of piles	10
Pier Pile Elements	EI (kN m^2)	4.3488×10^6

ρA (kg m^{-1})	8.4823×10^{3}
Pile length (m)	15
Number of piles (per pier)	4

The bridge is modelled as a 2D frame enabling longitudinal and vertical motion be considered, with the limitation that torsional and 'into the page' modes are excluded. This simplification is adopted for ease of programming the vehicle-bridge interaction (described in section 2.4), and because the relevant modes of interest are considered within a 2D frame-type system. The model is programmed in MATLAB using 6-degree-of-freedom (DOF) Euler-Bernoulli frame elements for the deck, abutments, pier and piles (Kwon and Bang 2000) and 2-DOF axial (spring) elements to model the lateral and vertical soil impedances. The various local mass and stiffness elements are assembled into global ($n \times n$) mass, **M** and stiffness, **K** matrices with a total of n = 861 DOFs (unscoured bridge). Damping is incorporated into the model using a Rayleigh approach (Clough and Penzien 1993, Yang et al. 2004), where the global damping matrix, **C** is assumed to be a linear combination of the **M** and **K** matrices. A damping ratio of 2% is assumed (Prendergast et al. 2017). The dynamic response of the bridge model can be obtained by solving Eq. (1), using the Wilson-Theta integration scheme (Tedesco et al. 1999, Dukkipati 2009).

$$\mathbf{M}\ddot{\mathbf{x}}(t)+\mathbf{C}\dot{\mathbf{x}}(t)+\mathbf{K}\mathbf{x}(t)=\mathbf{F}(t) \quad [1]$$

where $\mathbf{x}(t)$, $\dot{\mathbf{x}}(t)$ and $\ddot{\mathbf{x}}(t)$ denote the displacement, velocity and acceleration at each DOF for each time step and $\mathbf{F}(t)$ describes the external forces acting on each degree of freedom. In this paper, $\mathbf{F}(t)$ is populated using both ambient and vehicle-induced vibration – see Fig. 2. Details of the loading are presented in section 2.4.

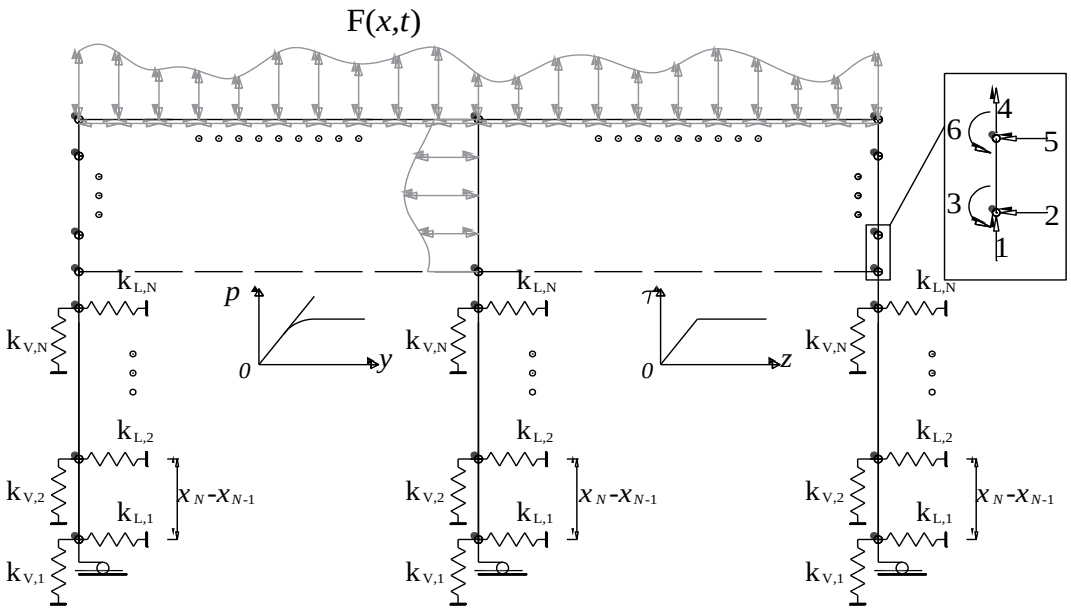

(a)

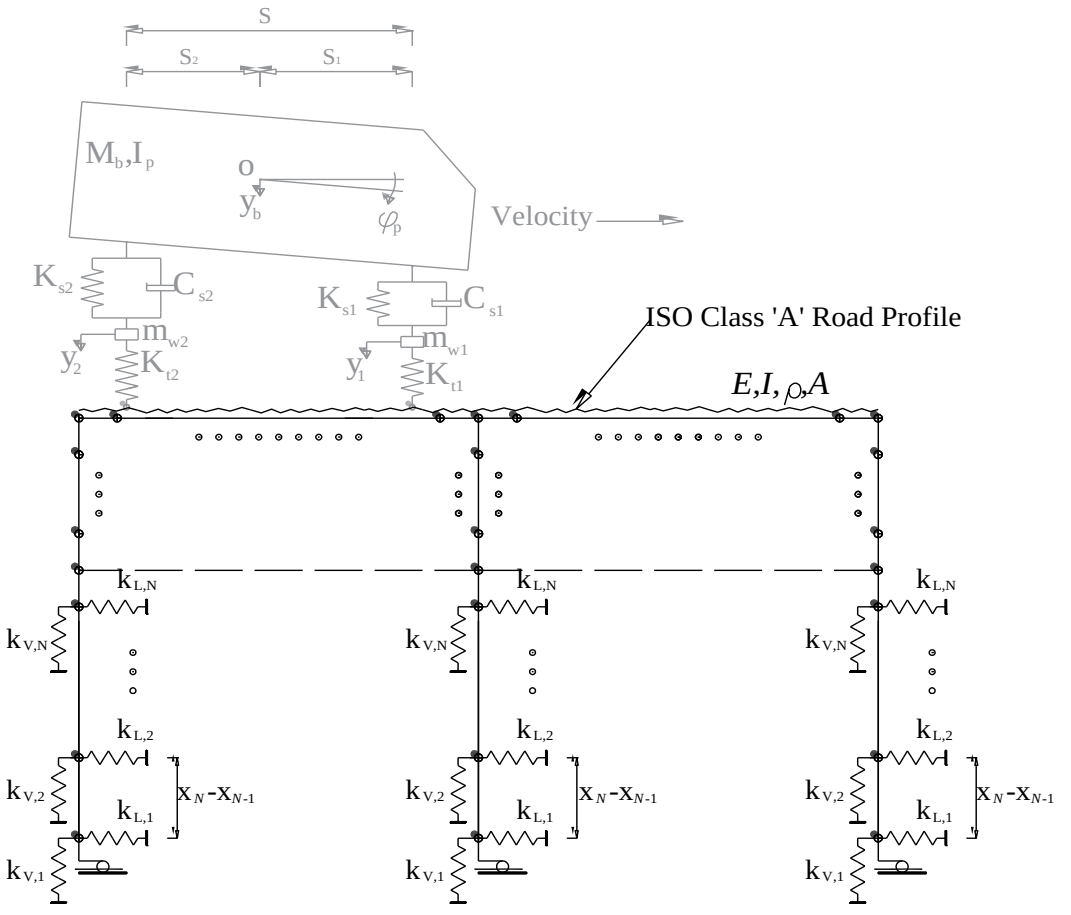

(b)

Fig. 2. Numerical schematic of bridge, (a) Ambient loading model, (b) Vehicle loading model

157 **2.2 Soil-foundation model**

158 The soil-structure interaction is modelled using Winkler springs (Winkler 1867, Dutta and Roy
159 2002), whereby the soil impedances are idealised as 2-DOF springs attached to the frame
160 elements for the piles – see Fig. 2. The stiffness of the soil is equivalent to a medium dense
161 sand, the properties of which are derived from the American Petroleum Institute design code
162 (API 2007). Both lateral load-displacement, *p-y* and vertical shear stress-displacement, *τ-z*
163 springs are modelled – see Fig. 2. Small-strain soil behavior is assumed in this paper, as it is
164 anticipated that the loading from environmental and vehicular sources will not induce large-
165 strain soil deformations. Therefore only the initial stiffnesses of the respective *p-y* and *τ-z*
166 curves are modelled, see Prendergast et al. (2017).

167 An Eigenvalue analysis is carried out using mass and stiffness matrices in the FE model of the
168 whole structure to obtain the bridge modal parameters (Clough and Penzien 1993). The bridge
169 first two natural frequencies are 1.43 Hz and 5.61 Hz. The first two mode shapes of the bridge
170 are shown in Fig. 3.

171

172

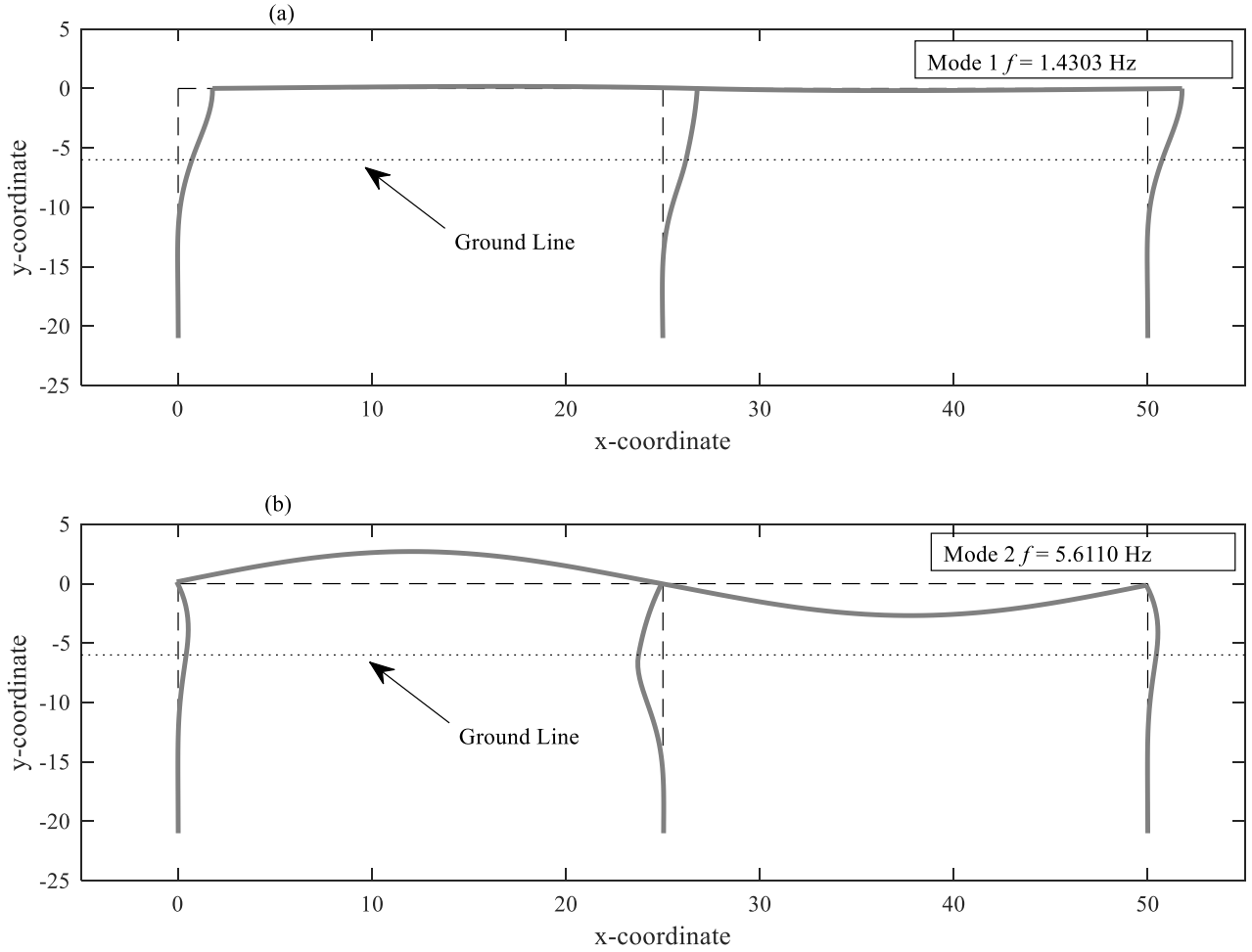

Fig. 3. The first two mode shapes of the unscoured bridge.

2.3 Scour modelling

The scour process is modelled by iteratively releasing vertical and horizontal springs (in pairs) from around the central pier foundation, commencing with those nearest the top. This corresponds to an increase in scour depth equivalent to the Finite Element (FE) discretization length, $x_N - x_{N-1}$, taken as 0.5 m in the present study – see Fig. 2.

183 **2.4 Load modelling**

184 Two types of loading are considered in this paper, ambient environmental loading and vehicle
185 induced loading. Both are described separately herein.

186 **2.4.1 Ambient loading**

187 Ambient loading is modelled as White Gaussian Noise (WGN) applied to the vertical and
188 horizontal DOFs of the bridge deck and the horizontal DOFs of the bridge pier. It is assumed
189 that no environmental loading is applied to the abutments as these are taken to be encased in
190 sleeves (Prendergast et al. 2017). A WGN signal is generated using an in-built function in
191 MATLAB and is subsequently scaled so that the majority of the loading occurs between ±100
192 N. This is undertaken to model low-level ambient excitation to the structure. The premise is
193 that if the approach can work under an arbitrarily low external excitation, then it has a higher
194 chance of success under larger loading incurred during windy conditions. Fig. 2(a) shows a
195 schematic of the ambient loaded model. Fig. 4(a) shows an example of a typical WGN signal
196 and Fig. 4(b) shows the distribution of the generated white noise, applied to one of the model
197 DOFs.

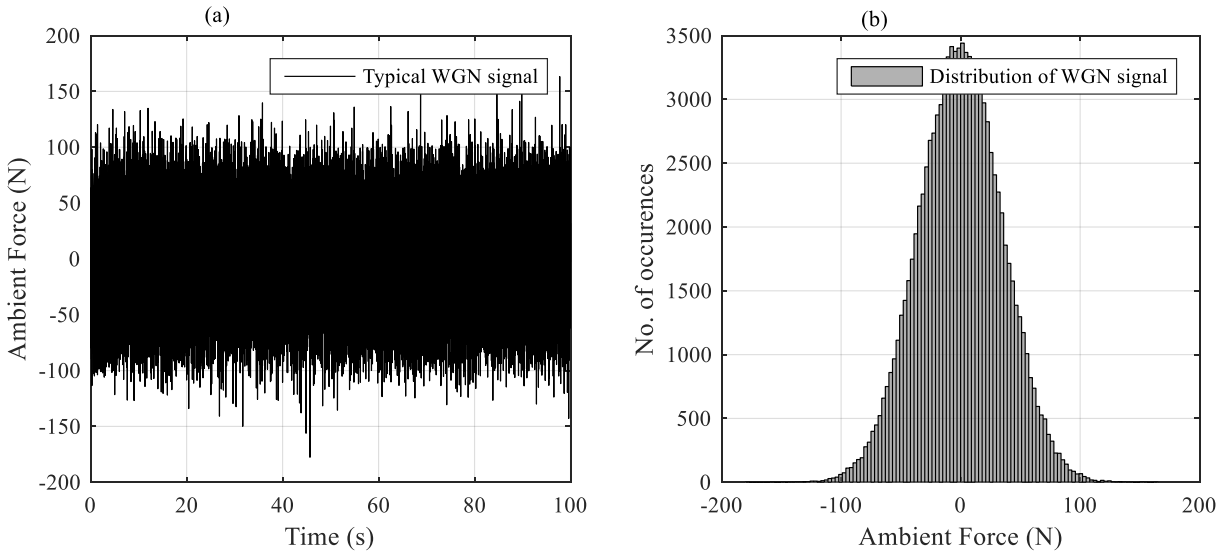

198

199 Fig. 4 Typical WGN signal as applied in bridge model (a) Time-series of signal, (b) Histogram of
200 signal shown in (a)

201 **2.4.2 Vehicular loading**

202 The vehicle model, see Fig. 2(b), is a two-axle truck that traverses the bridge deck. The model
203 is the same as that presented in Prendergast et al. (2016a, 2017) and similar to that in Hester
204 and González (2012) and González and Hester (2013). The reason for modelling a truck is to
205 ascertain if sufficient excitation of the relevant modes can be obtained by a passing vehicle and
206 to further investigate if the method postulated in this paper is adversely influenced by vehicle-
207 induced effects in the response spectra. In relation to the types of vehicle-induced effects that
208 can occur, elements of the forcing function may appear in the output signals. For example, the
209 rate at which a vehicle crosses a bridge may create a frequency peak in the response output,
210 and this can lead to issues with accurately tracking response features changing as a result of
211 damage. Fig. 2(b) shows that the vehicle has four DOFs, namely a vertical body bounce (y_b), a
212 body pitch (φ_p), and both front and rear axle hops (y_1 and y_2). The vehicle body is supported
213 on a suspension/axle assembly with a mass m_b and a rotational inertia I_p. The axle assemblies
214 have masses, m_{w1} and m_{w2} for the front and rear axles respectively. The stiffness coefficients of

the axle suspension systems are, K_{s1} and K_{s2}, respectively and they have damping coefficients, C_{s1} and C_{s2}, respectively. The front and rear tyres are modelled using linear springs with stiffnesses K_{t1} and K_{t2} respectively. The properties of the vehicle are outlined in Table 2.

Table 2. Parameters of vehicle model (Prendergast et al. 2017)

Parameter	**Property**	**Value**
Dimensions (m)	Wheel base (S)	5.5
	Dist from centre of mass to front axle (S_1)	3.66
	Dist from centre of mass to rear axle (S_2)	1.84
Mass (kg)	Front wheel/axle mass (m_{w1})	700
	Rear wheel/axle mass (m_{w2})	1,100
	Sprung body mass (m_b)	13,300
Inertia (kg m^2)	Pitch moment of inertia of truck (I_p)	41,008
Spring stiffness (kN m^{-1})	Front axle (K_{s1})	400
	Rear axle (K_{s2})	1000
Damping (kN s m^{-1})	Front axle (C_{s1})	10
	Rear axle (C_{s2})	10
Tyre stiffness (kN m^{-1})	Front axle (K_{t1})	1,750
	Rear axle (K_{t2})	3,500

By imposing equilibrium of the various forces and moments acting on the vehicle masses, the equations of motion can be obtained. Expressing these in terms of the vehicle DOFs enables the formulation of the (4×4) vehicle mass matrix $\mathbf{M_v}$, damping matrix $\mathbf{C_v}$ and stiffness matrix $\mathbf{K_v}$. The dynamic response of the vehicle as it traverses the bridge can be modelled as in Eq. (2).

$$\mathbf{M_v}\begin{Bmatrix}\ddot{\varphi}_p(t)\\ \ddot{y}_b(t)\\ \ddot{y}_1(t)\\ \ddot{y}_2(t)\end{Bmatrix}+\mathbf{C_v}\begin{Bmatrix}\dot{\varphi}_p(t)\\ \dot{y}_b(t)\\ \dot{y}_1(t)\\ \dot{y}_2(t)\end{Bmatrix}+\mathbf{K_v}\begin{Bmatrix}\varphi_p(t)\\ y_b(t)\\ y_1(t)\\ y_2(t)\end{Bmatrix}=\mathbf{F_v} \quad [2]$$

where $\mathbf{F_v}$ is the vector of forces acting on the vehicle degrees of freedom for each time step. The vehicle is programmed to commence motion over an approach distance of 100 m from the beginning of the bridge, to ensure that the initial vehicle conditions (pitch, displacements, etc.) as it enters the bridge are more realistic, and also to reduce the influence of initial transients in the signal resulting from the Wilson-Theta integration. As the vehicle traverses the bridge, it is excited by the presence of a road profile, which represents the roughness of the highway surface. In a vehicle-bridge interaction problem, the vehicle model and the bridge model interact dynamically through the contact forces between the deck and the vehicle wheels in a coupled and time-dependent manner (Yang et al. 2004). This means that the vehicle excites the bridge as it traverses, and the bridge vibration subsequently excites the vehicle. It is necessary that the contact forces between both sub-systems be the same to ensure compatibility. In this paper, an iterative approach to solve both dynamic sub-systems and maintain compatibility is adopted (Yang and Fonder 1996, Green and Cebon 1997). Solving Eq. (2) using the Wilson-Theta integration scheme enables calculation of the axle displacements y_1 and y_2 due to excitation from the road surface (including bridge displacements in the iterative solution). This enables calculation of the contact forces using Eq. (3) to be applied to the bridge. Application of the axle loads to the bridge is achieved by populating Eq. (1) using the Hermitian shape functions, which distribute the axles loads $F_1(t)$ and $F_2(t)$ as nodal forces and moments to the bridge deck elements.

$$\begin{Bmatrix} F_1(t) \\ F_2(t) \end{Bmatrix} = \begin{bmatrix} K_{t1} & 0 \\ 0 & K_{t2} \end{bmatrix} \begin{Bmatrix} y_1(t) \\ y_2(t) \end{Bmatrix} \quad [3]$$

For the analysis in this paper, the vehicle traverses an ISO Class 'A' road surface topography, which is generated according to Cebon (1999). This road surface is representative of a well-maintained highway.

3. Scour detection

3.1 Mode shape ratio (MSR) as a scour indicator

The mode shapes of the bridge contain valuable information about the bridge dynamic behavior. It can be seen in Fig. 3(a) that the first mode shape has high amplitudes in the horizontal direction at the top of the pier, whereas the second mode (Fig. 3b) has no amplitude at this location. For the purpose of detecting changes in modal behavior due to scour of the central pier, meaningful information relating to the pier dynamics can be obtained from the first mode of the bridge alone. This is because in flexible-abutment type two-span integral bridges, the central pier is generally a large stiff element, which provides lateral stability to the structure. Changing the boundary conditions of this element (due to scour at the foundation) alters the dynamic response of the full system and manifests as a change in global modal properties.

MSR is defined as the ratio of the modal amplitude at two points on the structure. The modal amplitude of the first mode shape is $\mathbf{\Phi_1} = [\phi_{11} \quad \phi_{12}]$, where ϕ_{11} and ϕ_{12} are the components (amplitudes) of the first mode shape at two points on the structure. For the purpose of detecting pier scour, the first point is taken as the (vertical) modal amplitude at the mid-span of the left-hand side span, and the second point is taken as the (horizontal) modal amplitude at the top of the pier (S_1 and S_2 in Fig. 1), and MSR is obtained as in Eq. (4).

$$MSR = \frac{\phi_{11}}{\phi_{12}} \quad [4]$$

The influence of scour erosion around the central pier on the MSR is investigated to determine its sensitivity to changes in foundation stiffness in integral-type bridge structures. Fig. 5 provides a visualization of these mode shapes for zero and 5 m scour of the pier, as determined by solving of the Eigen-problem (Clough and Penzien 1993). Fig. 5(a) shows the first mode shape of the bridge for zero and 5m scour. Fig. 5(b) shows the zoomed in view at the top of the pier, which shows the differences in the modal amplitudes more clearly. As is evident by the differences in (absolute) modal displacements, it can be expected that the MSR for zero scour will be different to that for the 5 m scour case, due to the difference in magnitude of the deck mode component between the plots.

To demonstrate this, the MSR obtained by implementing scour in the model in steps of 0.5m at the central pier foundation, is shown in Table 3. Scour is modelled by successively removing springs from the central pier piled foundation corresponding to increases in scour depth.

Table 3. Change in MSR under pier scour from eigenvalue analysis on model

Scour (m)	**MSR**	**% Change from zero scour**
0	0.095	0
0.5	0.094	-1.1
1	0.091	-4.2
1.5	0.086	-9.5
2	0.082	-13.7
2.5	0.076	-20.0
3	0.071	-25.3
3.5	0.065	-31.6
4	0.059	-37.9
4.5	0.0537	-43.5
5	0.0484	-49.1

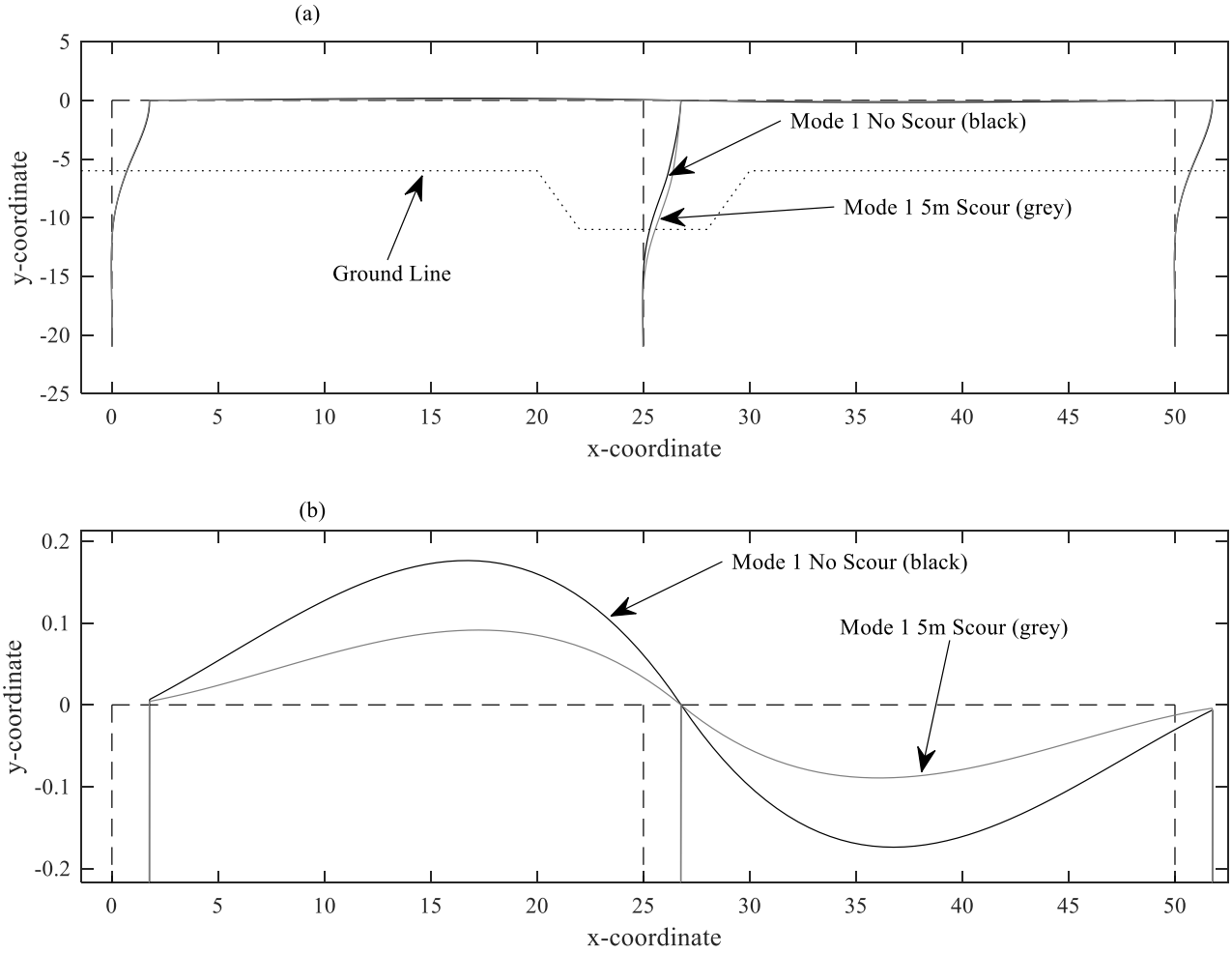

Fig. 5 The change of the first mode shape due to scour, (a) full view, (b) zoomed view at deck level.

3.2 Identification of bridge mode shapes in time-domain

The data in Table 3 and Fig. 5 is generated from an eigenvalue analysis in the numerical model to demonstrate the MSR approach. However, on a real bridge, mode shape information will have to be obtained using time-domain measurements from a sensor on the structure. In this paper, ambient and vehicular excitation are modelled and the MSR is derived from mode shapes obtained by analysis of the resulting dynamic signals, to remain physically in keeping

with the placement of accelerometers on a test structure. The method for obtaining the modal information is outlined herein.

Output-only modal identification aims at identifying the modal parameters (frequencies, damping ratios and mode shapes) of a structure using only the responses from the system where the excitation forces are unknown (Brincker and Ventura 2015). In this paper, Frequency Domain Decomposition (FDD) (Brincker et al. 2000) is employed to find the frequencies and mode shapes of the structure from time-domain data. It should be noted that other output-only modal identification procedures can also be used. Acceleration responses are calculated at three virtual node points ('sensors') by solving Eq. (1). Sensor S1 is the vertical acceleration measured at the mid-point of the left-hand span, sensor S2 is the lateral (horizontal) acceleration measured near the top of the pier (in the traffic direction) and sensor S3 is the vertical acceleration measured at the mid-point of the right-hand span – see Fig. 1. FDD begins by estimating the power spectral density matrix, $\hat{\mathbf{G}}_{\mathbf{yy}}(j\omega)$ of the various responses at discrete frequencies, $\omega = \omega_i$. $\hat{\mathbf{G}}_{\mathbf{yy}}(j\omega)$ is decomposed at each discrete frequency by applying Singular Value Decomposition (SVD) (Brincker et al. 2000) – see Eq. (5):

$$\hat{\mathbf{G}}_{\mathbf{yy}}(j\omega) = \mathbf{U_i}\mathbf{\Sigma_i}\mathbf{U_i^H} \quad [5]$$

where $\mathbf{U_i}$ is the unitary matrix of singular vectors and $\mathbf{\Sigma_i}$ is a diagonal matrix holding the singular values. The superscript 'H' denotes the complex conjugate of the matrix and $j = \sqrt{-1}$. A SVD diagram is plotted using the singular values obtained at each discrete frequency. Dominant peaks of the SVD diagram are natural frequencies and the corresponding singular vectors are mode shapes.

4. Performance of frequency and MSR as scour indicators

In this section, the performance of the MSR technique at monitoring pier scour is investigated and benchmarked against the more established natural frequency approach. Both ambient loading and vehicle-induced loading are studied to test the resilience of the MSR approach. As real sensors will contain noise, artificial noise is also added to study its effect on the accuracy of the method, as discussed herein.

4.1 Results under ambient loading

White Gaussian Noise is used to generate low-level forces with peak magnitude of the order of ±100 N to simulate environmental excitation, and this is applied to the horizontal and vertical DOFs of the bridge deck and the horizontal DOFs of the pier. It is assumed that the flexible abutment columns are not subjected to this ambient loading due to being encased in sleeves (see Prendergast et al. (2017) for modelling information). Acceleration responses due to this excitation are calculated at S1 and S2 by solving Eq. (1) – see Fig. 6(a). FDD is applied to these output acceleration responses and the SVD diagram is plotted in Fig. 6(b). A peak at 1.419 Hz is detected corresponding to the first mode of the bridge (see Fig. 3(a) for a view of the first mode of the bridge – global sway). The MSR is obtained from the singular vector corresponding to this frequency.

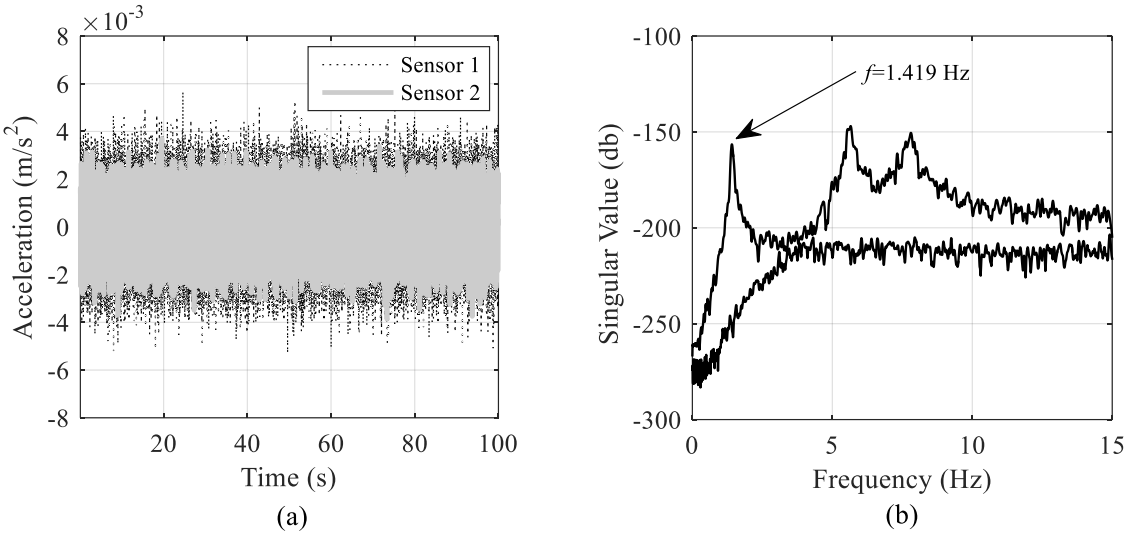

337

338 Fig. 6 Responses to ambient loading, (a) Acceleration responses at S1 and S2, (b) SVD
339 diagram obtained from these accelerations.

340

341 From Table 3, it is expected that 5m central pier scour will lead to approximately 50% reduction
342 in MSR value (as derived from the Eigenvalue analysis). In this section, the ability for the MSR
343 to be reliably extracted for the same scour conditions when the bridge is subjected to ambient
344 loading data is investigated. A series of scour depths affecting the central pier foundation are
345 modelled, from 0 m to 5 m in increments of 0.5 m. The natural frequencies and MSRs for each
346 case are estimated using FDD applied to the accelerations generated at the sensor nodes. Both
347 noise-free signals and contaminated signals are examined. The contaminated signals contain a
348 Signal-to-Noise Ratio (SNR) of 20, equating to 5% noise interference. This noise is added to
349 the unpolluted signals generated in the numerical model using a procedure described in Lyons
350 (2011) and Prendergast et al. (2016b). The estimated frequencies of the bridge plotted against
351 scour depth are shown in Fig. 7(a). The noise-free natural frequency reduces from 1.419 Hz for
352 zero scour to 1.137 Hz as the scour depth increases to 5m at the pier. The MSRs estimated from
353 FDD for these scour depths are shown in Fig. 7(b). It can be seen that the noise-free MSR

reduces from 0.0978 for the healthy bridge to 0.0477 when there is 5m scour. The noisy signals follow the same trend for both cases.

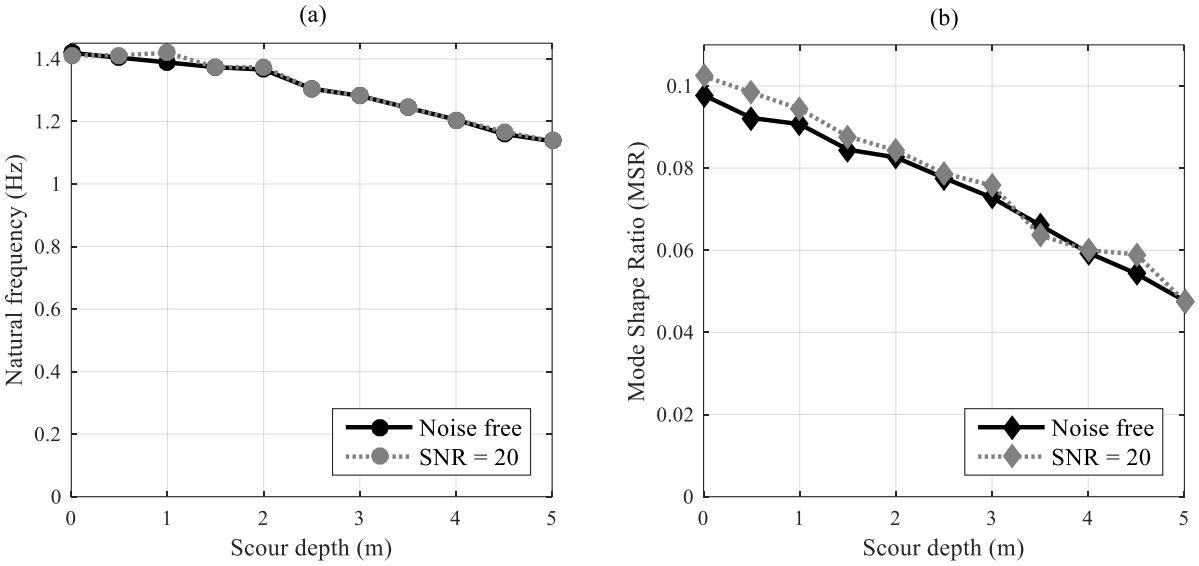

Fig. 7 Modal parameters of the bridge in presence of scour from ambient vibrations, (a) Natural frequency, (b) MSR

The results in Fig. 7 highlight the sensitivity of both the natural frequencies and the MSR to progressive scour at the central pier. It can be seen that while the natural frequency reduces by approximately 20% from the healthy (unscoured) case to the 5 m deep scour case, the MSR decreases by more than 50% for the same level of scour. This suggests that the MSR may be a more scour-sensitive damage indicator than the commonly adopted natural frequency, for the case considered here.

4.2 Results under vehicle loading

Although ambient excitation can be obtained from sources such as wind, these sources may not provide sufficient excitation and hence, resolution accuracy. Vehicle-induced vibration is

another source of operational excitation on road/rail bridges (Farrar et al. 1999), though this type of excitation can induce vehicle and loading related frequencies into the response spectra. A two-axle vehicle (truck model) is simulated in this paper to pass over a Class 'A' road surface on the bridge at a speed of 30 km/h (Fig. 2b) to create the required input excitation (see Table 2 for vehicle properties). The acceleration responses of the bridge are calculated at sensor locations S1 (vertical) and S2 (horizontal), see section 2.4.2 for details on modelling. The free vibration part of the responses when the vehicle leaves the bridge are considered in the analysis as shown in Fig. 8(a), to reduce the influence of the vehicle forcing frequencies – see Prendergast et al. (2017) for a study on the type of vehicle-related interference that can occur. Note, while only 20 seconds worth of signal are shown in Fig. 8(a) for clarity, a signal length of 40 seconds is actually analyzed. A similar procedure as described previously is applied to the acceleration responses to obtain the frequencies and MSR at each scour depth. Fig. 8(b) shows the SVD diagram obtained from FDD. There is a peak detected at 1.434 Hz corresponding to the first mode of the bridge (global sway – see Fig. 3(a)).

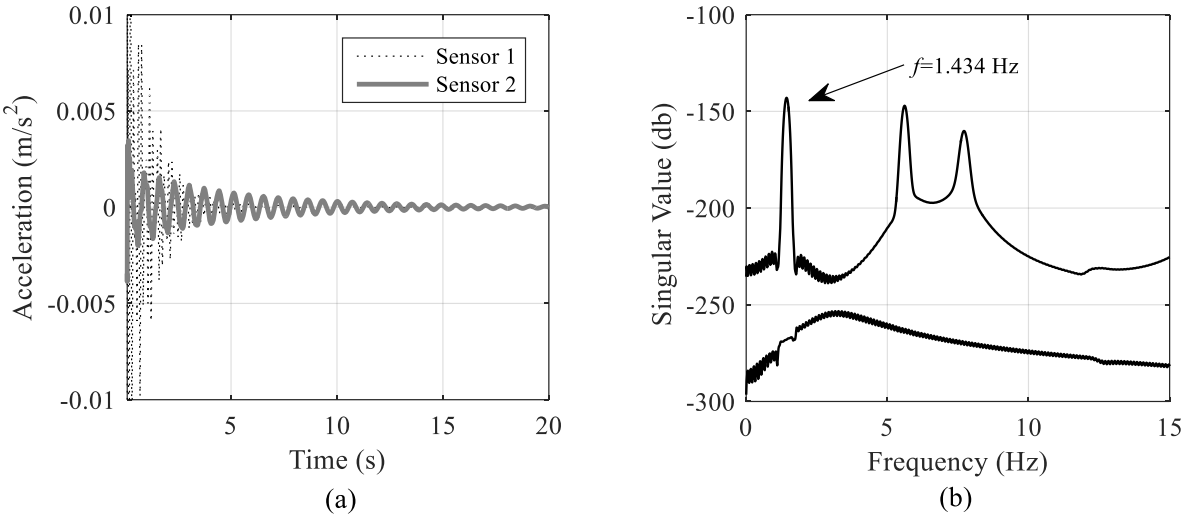

Fig. 8 (a) Free vibrations at S1 and S2 after vehicle passes at 30km/h, (b) SVD diagram

Scour depths ranging from 0 to 5 m at the pier are considered, in increments of 0.5 m as undertaken previously. The natural frequencies and MSRs estimated from FDD are shown in Figs. 9(a) and (b), respectively, for both noise-free and contaminated signals (SNR=20). The noise addition process is the same as undertaken previously (Lyons 2011). The percentage change in natural frequency in Fig. 9(a) follows a similar trend as that obtained for ambient vibrations, showing approximately 20% change over 5 m scour. The overall change in MSR is also similar to the previous (ambient) case, but the plot is not as smooth, which may be a function of the shorter time signals used for the vehicle-loaded case (40 seconds) versus the ambient case (100 seconds). Also, it has been shown in previous studies that the quality of the acceleration signals measured on a bridge can be affected by interaction effects between the vehicle and the bridge such as the variation of vehicle velocity relative to the natural period of the bridge (Prendergast et al. 2016b). These interaction effects can magnify and diminish the response amplitude in subsequent free vibration by influencing the initial displacement, velocity and acceleration conditions at the beginning of the free vibration.

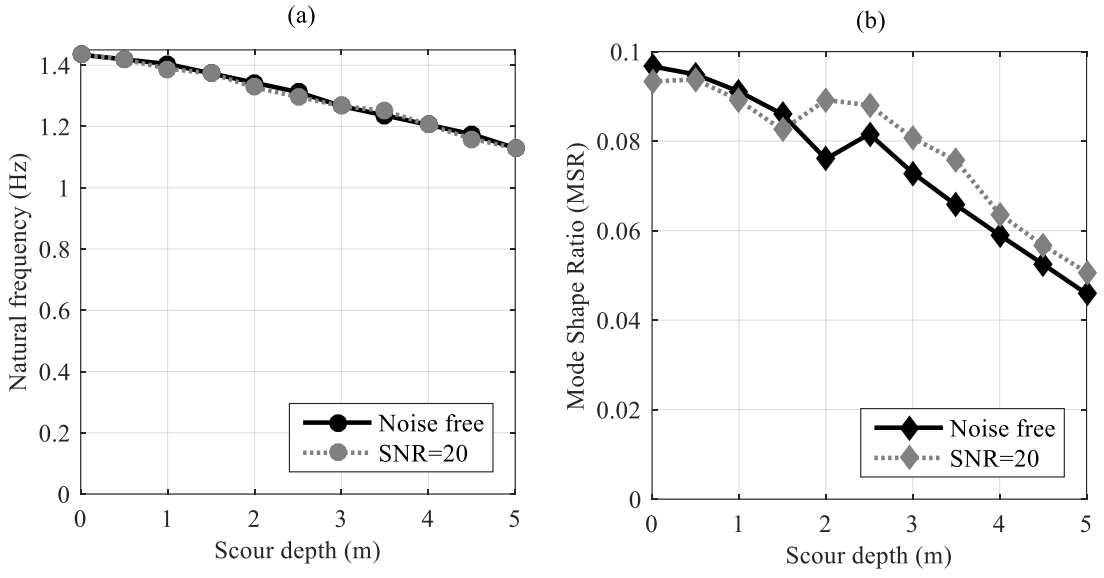

Fig. 9 Modal parameters of the bridge in the presence of scour from vehicle-induced vibration, (a) Natural frequency, (b) MSR

Due to the potential for vehicle-bridge interaction related pollution of the response data, all subsequent analyses are conducted under ambient vibration conditions only.

4.3. Effect of bridge deck dimensions on MSR technique

It is shown in previous sections that the first mode shape of the two-span integral bridge investigated in this paper is sensitive to scour at the pier in that the modal amplitude of the deck changes significantly under scour. To ensure that this is not simply due to its particular geometry, a brief investigation is conducted herein. The sensitivity of the MSR to the bridge span length is studied by developing two further bridge models, the first with two spans of lengths 20m and the second with two spans of length 30m. The procedure to develop these models is the same as that applied to create the 2 × 25m span model used throughout this paper, and relevant design considerations have been adhered to in the development (Concast 2014). The first global mode shape of each model is identified using an Eigenvalue analysis on the respective mass and stiffness matrices. The MSR values for the healthy and 5m scour cases for each of the three bridge models are given in Table 4.

Table 4. Change in MSR values for three 2-span bridge geometries under 5m pier scour

Span length (m)	20	25	30
	MSR		
No scour	0.063	0.096	0.137
5 m scour	0.032	0.048	0.07
% Change	-49.2	-50	-48.9

Table 4 shows that the value of MSR decreases when the span length increases for a given scour condition. In all cases, however, there is approximately 50% reduction in the MSR when there is 5m scour at the pier relative to the no scour values. This brief analysis suggests that the proposed MSR method can be successfully employed for two-span integral bridges of various (typical) span lengths.

An expansion of the approach to three-span integral bridges did not provide satisfactory results. Three-span bridges have two central piers, and the asymmetry of scour affecting one of the two central piers leads to inconsistent changes in MSR. Furthermore, for symmetrical three-span bridges, the central span exhibits very low modal amplitude at its mid-point meaning that deriving MSR using this point is subject to significant errors.

5. Combined frequency and MSR measurements under changing temperature conditions

Temperature changes in the environment occur naturally on both a diurnal and annual basis, leading to changes in ambient air temperature and therefore, the operational temperature of structures. In this section, the effect of a change in temperature on the performance of the scour monitoring approach is investigated.

Changes in environmental temperature can affect the material properties of structures, which can subsequently alter dynamic properties (Sohn 2007). The frequency of vibration of a structure can be significantly affected by temperature changes, which may pose issues for frequency-based SHM regimes. There is significant uncertainty surrounding this topic. For example, the correlation between the temperature of the air and the internal temperature of a bridge element can be uncertain, and is affected by whether the air temperature is constant, rising, or falling. Applying a correction factor for temperature is, therefore, not so trivial, and

moreover there is little guidance given in the literature on the magnitude of the influence of temperature on material stiffness. In fact, what literature does exist gives widely varied results, which can differ by more than 100% (Žnidarič et al. 2013). In this section, a simple model is adopted to alter the material properties of a bridge with a view to testing the combined MSR and frequency approach. The method of accounting for temperature is to alter the elastic modulus of concrete at various components of the bridge (Limongelli 2010). This is undertaken using Eq. (6) (Žnidarič et al. 2013).

$$E_k = E_0\left(1+\beta\Delta T\right) \quad [6]$$

where E_0 is the elastic modulus at reference temperature T_0 (unaltered situation), E_k is the elastic modulus at temperature T_k (altered situation), β is the thermal hardening coefficient ($°C^{-1}$), taken as -0.0118 (Kassir et al. 1996) and $\triangle T$ is the change in temperature (T_k - T_0). The reference temperature is taken as T_0=10°C. Maximum and minimum air temperatures of 28°C and 16°C respectively are arbitrarily assumed, with effective concrete temperature varying from air temperature according to the Eurocode (CEN 2003). Note, the calculation for converting air temperature to effective concrete temperature may only be valid for extreme cases, but is adopted herein for the sensitivity study. An effective deck and pier temperature of 26.5°C is assumed (average effective concrete temperature). The abutments are assumed to be at a temperature between soil temperature (assumed as 12°C) and effective concrete temperature, giving just over 19°C. The piles are assumed not to change temperature from T_0. The results of applying Eq. (6) to the various bridge components yields the modified elastic moduli as outlined in Table 5.

Table 5. Modified elastic modulus at various points of bridge model due to temperature

Element	**Material**	E_0	β	T_0	T_k	ΔT	E_k	**Change**
		(N m^{-2})		(°C)	(°C)	(°C)	(N m^{-2})	%
Deck	Concrete	35×10^9	-0.0118	10	26.5	16.5	28.2×10^9	-19.47
Pier	Concrete	35×10^9	-0.0118	10	26.5	16.5	28.2×10^9	-19.47
Abutment	Concrete	35×10^9	-0.0118	10	19.25	9.25	31.2×10^9	-10.92

Eq. (6) yields a 19.5% reduction in the elastic modulus of the deck and pier, and an 11% reduction in the elastic modulus of the abutments. Note that these changes may not be realistic but are adopted to represent the case where the bridge is subjected to a temperature gradient and the resulting effect on the extracted dynamic properties for scour detection is evaluated.

An analysis is conducted to quantify the relative effects of the arbitrary increase in temperature described above on 'measured' frequency and MSR values for a range of scour conditions. This is carried out under ambient loading only, as the vehicle loading introduces its own natural errors, as shown previously. To check the effect of the change in these material parameters due to temperature, 10 runs of the ambient load model are undertaken (with newly generated WGN ambient loading in each run) for scour depths of the central pier ranging from 0 m to 5 m in 0.5 m increments. No noise is considered in this initial trial and the results are presented in Fig. 10. Fig. 10(a) shows the average frequency measured at each scour depth, as well as the individual frequency results at each depth for each of the ten runs, shown as circles for the original temperature and diamonds for the altered temperature cases. Fig. 10(b) shows the average MSR measured at each depth for both temperature conditions, as well as the results for individual runs shown as crosses for the unaltered temperature and squares for the altered

487 temperature. The variation in detected frequency and MSR for each run is due to the differences
488 arising from the random nature of the WGN loading for each run. The degree of this variation
489 is expressed in Table 6, which displays the coefficient of variation, COV (%) for the ten runs
490 at each scour depth for both frequency and MSR, under both temperature conditions.

491 Table 6. Variability in frequency and MSR for different runs and temperature conditions – no noise

T	**Scour Depth (m)**	**0**	**0.5**	**1**	**1.5**	**2**	**2.5**	**3**	**3.5**	**4**	**4.5**	**5**	**Max**
T_0	Avg. *f* (Hz)	1.434	1.426	1.395	1.367	1.336	1.305	1.272	1.237	1.194	1.166	1.129	
	COV (%)	0.6	1.1	1.5	0.8	0.8	0.8	1.1	1.3	0.7	0.9	1.0	1.5
T_k	Avg. *f* (Hz)	1.372	1.358	1.331	1.309	1.280	1.248	1.217	1.189	1.158	1.124	1.090	
	COV (%)	0.8	1.2	0.9	1.4	0.7	0.8	1.0	1.5	1.3	1.1	1.4	1.5
T_0	Avg. MSR	0.097	0.095	0.092	0.089	0.083	0.077	0.072	0.066	0.060	0.055	0.049	
	COV (%)	1.7	1.7	1.1	1.6	1.9	1.5	1.6	1.6	1.8	2.3	1.6	2.3
T_k	Avg. MSR	0.105	0.103	0.101	0.095	0.090	0.085	0.078	0.072	0.065	0.061	0.055	
	COV (%)	2.1	1.8	1.6	1.6	1.5	1.7	1.6	1.7	2.9	2.6	3.1	3.1

492

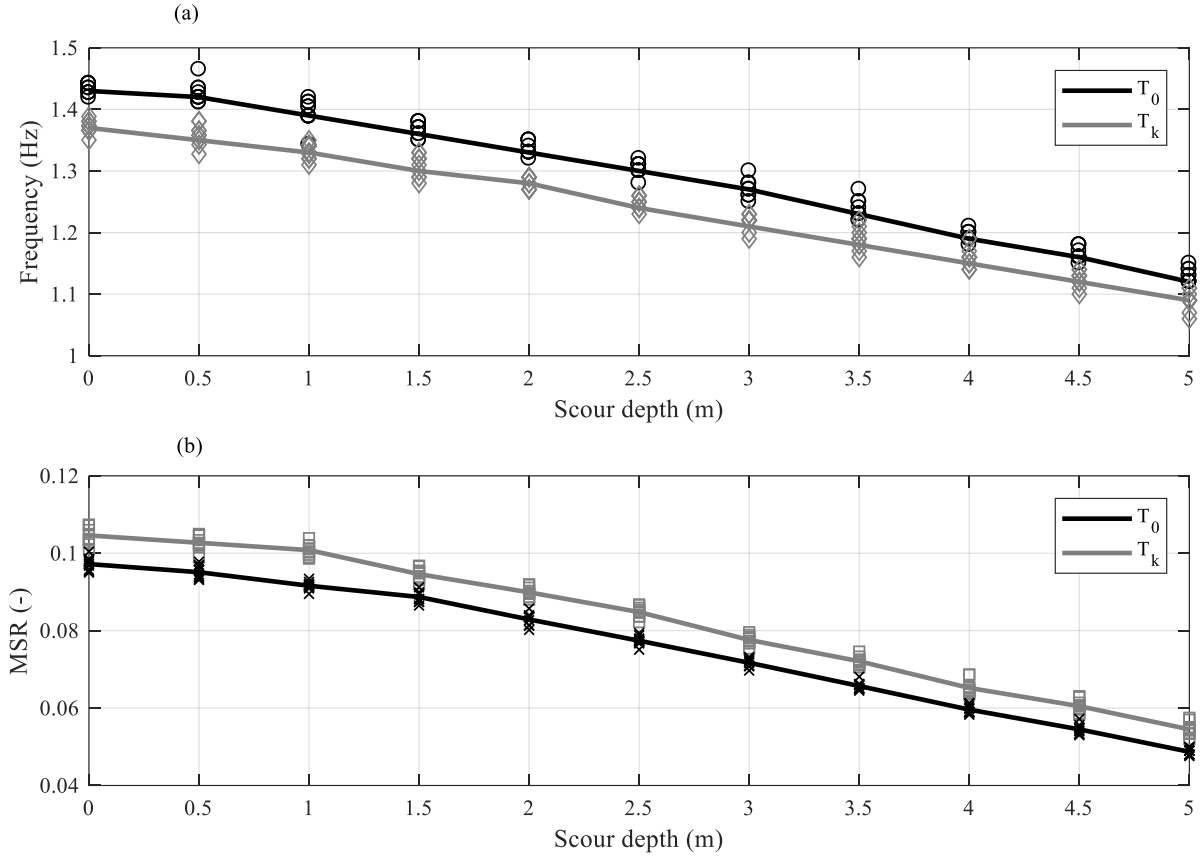

493

494 Fig. 10 Effect of temperature change on scoured parameters (a) average frequency with
495 individual runs (circles and diamonds), (b) average MSR with individual runs (crosses and
496 squares)

497

498 Observing Fig. 10 and Table 6, two particular points become evident. Firstly, the degree of
499 variation in the measured MSR for the ten runs at each scour depth is greater than that of the
500 detected frequency, with a maximum COV of 3.1% versus 1.5%. This variability suggests that
501 MSR may be sensitive to the random variations in loading, as this is in effect the only difference
502 between each analysis run at a given scour level. This was already evident from the somewhat
503 untidy results from the vehicle-induced loading case (see Fig. 9), which had a moderately
504 detrimental effect on the MSR approach. Secondly, the effect of a temperature increase is to
505 *decrease* the measured average frequency, whereas the average MSR experiences an *increase*.
506 The mean percentage change in average frequency between original and modified temperature

for all scour depths equated to -4.1% (with maximum and minimum changes of -4.8% and -3%), whereas the mean percentage change in average MSR between both temperatures and for all scour depths equated to +9.2% (with maximum and minimum changes of 11.9% and 6.7%).

The analysis in Fig. 10 and Table 6 was conducted in the absence of noise pollution of the signals. Table 7 shows the same results as Table 6 but for signals containing SNR=20. For these cases, the degree of variation increases somewhat. For example, the maximum COV in frequency measurements increases from 1.5% in the absence of noise to 2.3% with added noise. Similarly, the maximum COV in MSR measurements increases from 3.1% without noise to 16.4% with added noise. The mean percentage change in average frequency between original and modified temperature including noise for all scour depths equated to -3.8% (with maximum and minimum changes of -4.6% and -2.9%), and the mean percentage change in average MSR between both temperatures (with noise) and for all scour depths equated to +11% (with maximum and minimum changes of 19.6% and 4.8%). These results indicate that although noise increases the variability in the results, the trend of frequency decreasing and MSR increasing under increased temperature remains.

Table 7. Variability in frequency and MSR for different runs and temperature conditions – with noise

T	**Scour Depth (m)**	**0**	**0.5**	**1**	**1.5**	**2**	**2.5**	**3**	**3.5**	**4**	**4.5**	**5**	**Max**
T_0	Avg. f (Hz)	1.441	1.418	1.398	1.373	1.347	1.308	1.273	1.234	1.202	1.167	1.135	
	COV (%)	1.4	0.7	1.2	0.7	0.8	0.8	1.3	1.2	1.0	0.6	0.8	1.4
T_k	Avg. f (Hz)	1.376	1.358	1.349	1.320	1.286	1.262	1.224	1.189	1.167	1.125	1.096	
	COV (%)	2.3	1.0	1.0	0.9	1.4	0.9	1.0	0.6	1.0	1.2	0.8	2.3
T_0	Avg. MSR	0.097	0.096	0.092	0.089	0.081	0.074	0.073	0.064	0.061	0.055	0.050	
	COV (%)	4.0	4.6	3.6	5.6	9.8	7.0	7.4	7.7	13.1	10.4	15.4	15.4
T_k	Avg. MSR	0.104	0.100	0.100	0.096	0.091	0.087	0.080	0.071	0.069	0.065	0.056	
	COV (%)	5.1	5.0	5.4	6.9	7.1	6.2	6.0	10.6	9.2	16.4	8.7	16.4

6. Discussion on applicability to real structures

In this section, some practical considerations related to applying the method to real structures is discussed. From a practical standpoint, acceleration measurements can be continuously taken over a period of time, and an average frequency and MSR can be established for a given structure to reduce the variation caused by the random loading and noise. For example, a given run of 1000 seconds can be divided into ten segments and the average values of the frequency and MSR can be established. If average frequency is observed to *decrease* between subsequent readings by a statistically significant amount, with a corresponding *decrease* in MSR, this may indicate the presence of scour. If average frequency is seen to *decrease* with a corresponding *increase* in MSR, this may indicate an increase in the structure's temperature. With relation to how much statistical significance is required, a trigger could be programmed to occur if a deviation exceeds the mean plus a portion of the standard deviation (Kullaa 2003, Fitzgerald et al. 2019b). These conditions are summarised in Table 8. Using the combined measurements in this manner may provide significantly more reliable information to an infrastructure manager, and potentially makes possible the removal of environmental (temperature) influences. Critically, this added benefit comes without a corresponding increase in sensor requirements as all the required information can be obtained from the same sensor network. The approach requires a minimum of two sensors and only output accelerations are used to derive the various parameters. It should be noted that for the case where scour occurrence coincides with an increase in temperature, there is potential for the scour effect to be masked since scour occurrence and temperature increasing both lead to reductions in frequency, but have opposite effects on MSR. Practically speaking this should not present as a major issue, since it is anticipated that changes in temperature will typically occur over relatively long time periods compared to scour, which tends to occur rapidly under flooded conditions.

549 Table 8. Matrix of likely causes of parameter changes

	Avg. MSR	Avg. Frequency	Likely cause
Change	decrease	decrease	scour
	increase	decrease	temperature increase
	increase	increase	scour refilling
	decrease	increase	temperature decrease

550

551 Some practical limitations persist, which require consideration. One issue relates to powering
552 of the sensors. Dynamic measurements are energy-intensive, and this remains a barrier to
553 widespread deployment of these systems. There have been some notable improvements in
554 recent years in sensor technology and energy harvesting, which are becoming practical (Cahill
555 et al. 2018, Fitzgerald et al. 2019a). Furthermore, it is anticipated that the method would work
556 best if a full modal study of the target structure is undertaken at the time of sensor deployment.
557 This would additionally involve a scour survey to understand the initial conditions affecting
558 the structure. This can be a labour-intensive exploit and may practically limit the amount of
559 bridges on a network that can be monitored.

560

561 ## 7. Conclusions

562 In this paper, a novel scour detection method based on Mode Shape Ratios between two sensor
563 locations on a two-span integral bridge structure is investigated, as a potential tool to mitigate
564 (in combination with frequency measurements) temperature influences from distorting
565 vibration-based scour results. The study builds on previous work based on natural frequency
566 measurements and proposes this approach which is more sensitive to the stiffness changes
567 induced by scour. The method is illustrated using numerical modelling of an integral bridge

568 loaded by ambient and vehicular loading. The MSR of two points on the deck and pier changes
569 by approximately 50% for 5 m of scour around the central foundation of the case study bridge
570 as opposed to a change in frequency of 20% for the same scour level.
571
572 While promising, the MSR has some drawbacks. It is generally sensitive to loading,
573 particularly to vehicle-bridge interaction effects, which induce some errors in the approach for
574 vehicle-induced vibrations. It is also sensitive to random errors due to ambient loading, leading
575 to some variation in calculated MSR for various model runs. Expansion of the approach to
576 abutment monitoring (using the first mode) was not possible, as the MSR was not sensitive to
577 changes induced in the global sway mode due to scour at these locations. Furthermore,
578 expansion to a three-span bridge did not yield a consistent trend.
579
580 However, for two-span integral bridges, if several runs are undertaken and the average MSR
581 and frequency (in combination) are derived, the method provides some significant additional
582 information on the nature of the scour conditions potentially affecting a structure. Both
583 frequency and MSR reduce with scour, while frequency reduces with increasing temperature.
584 MSR, however, increases with increasing temperature, meaning the temperature effect can be
585 separated from the scour effect when both measurements are combined. It should be noted of
586 course that a simplified temperature model was implemented and it is acknowledged that the
587 temperature variation in a real structure could be quite different. The analysis in this paper is
588 therefore undertaken to demonstrate that MSR and frequency exhibit an inverse relationship to
589 temperature variation, and this is potentially a useful characteristic.
590

591 Only scour damage was assumed in this paper. The effect of other damage types such as
592 corrosion or cracking were not assessed and may also influence the MSR results. The results
593 in this study are encouraging for scour measurements around integral-type bridge structures
594 and indicate the potentially useful addition of MSR to the frequency-based SHM approach.

595

596 Acknowledgements

597 The authors gratefully acknowledge Science Foundation Ireland for supporting this research
598 under the US/Ireland program.

599

600 References

601 API. 2007. API RP2A-WSD. *In* Recommended Practice for Planning, Designing, and
602 Constructing Fixed Offshore Platforms–Working Stress Design, American Petroleum
603 Institute, Washington, DC.

604 Avent, R.R., and Alawady, M. 2005. Bridge Scour and Substructure Deterioration : Case
605 Study. Journal Of Bridge Engineering, **10**(3): 247–254.

606 Bao, T., Andrew Swartz, R., Vitton, S., Sun, Y., Zhang, C., and Liu, Z. 2017. Critical insights
607 for advanced bridge scour detection using the natural frequency. Journal of Sound and
608 Vibration, **386**: 116–133. Elsevier. doi:10.1016/j.jsv.2016.06.039.

609 Briaud, J.L., Chen, H.C., Ting, F.C.K., Cao, Y., Han, S.W., and Kwak, K.W. 2001. Erosion
610 Function Apparatus for Scour Rate Predictions. Journal of Geotechnical and
611 Geoenvironmental Engineering,: 105–113.

612 Briaud, J.L., Hurlebaus, S., Chang, K., Yao, C., Sharma, H., Yu, O., Darby, C., Hunt, B.E.,
613 and Price, G.R. 2011. Realtime monitoring of bridge scour using remote monitoring
614 technology. *In* Security. Austin, TX. Available from http://tti.tamu.edu/documents/0-
615 6060-1.pdf.

616 Brincker, R., and Ventura, C.E. 2015. Introduction to Operational Modal Analysis. John
617 Wiley & Sons, Ltd, Chichester, UK. doi:10.1002/9781118535141.

618 Brincker, R., Zhang, L., and Andersen, P. 2000. Modal Identification from Ambient
619 Responses using Frequency Domain Decomposition. *In* Proceedings of 18th
620 International Modal Analysis Conference.

621 Brincker, R., Zhang, L., and Andersen, P. 2001. Modal identification of output-only systems
622 using frequency domain decomposition. Smart Materials and Structures, **10**(3): 441–
623 445. doi:10.1088/0964-1726/10/3/303.

624 Cahill, P., Mathewson, A., and Pakrashi, V. 2018. Experimental Validation of Piezoelectric
625 Energy-Harvesting Device for Built Infrastructure Applications. Journal of Bridge
626 Engineering, **23**(8): 04018056. doi:10.1061/(asce)be.1943-5592.0001262.

627 Cebon, D. 1999. Handbook of Vehicle-Road Interaction. Swets & Zeitlinger, Netherlands.

628 CEN. 2003. EN 1991-1-5 Eurocode 1: Actions on structures, Part 1-5: General actions -
629 Thermal actions.

630 Chang, K., and Kim, C. 2016. Modal-parameter identification and vibration-based damage
631 detection of a damaged steel truss bridge. Engineering Structures, **122**: 156–173.
632 Available from http://www.sciencedirect.com/science/article/pii/S0141029616301845
633 [accessed 31 May 2017].

634 Chen, C.-C., Wu, W.-H., Shih, F., and Wang, S.-W. 2014. Scour evaluation for foundation of
635 a cable-stayed bridge based on ambient vibration measurements of superstructure. NDT
636 & E International, **66**: 16–27. Elsevier. doi:10.1016/j.ndteint.2014.04.005.

637 Clough, R.W., and Penzien, J. 1993. Dynamics of structures.

638 Concast. 2014. Concast Precast Group. Available from
639 http://www.concastprecast.co.uk/images/uploads/brochures/Concast_Civil.pdf [accessed
640 1 May 2014].

641 Dukkipati, R.V. 2009. Matlab for Mechanical Engineers. New Age Science.

642 Dutta, S.C., and Roy, R. 2002. A critical review on idealization and modeling for interaction
643 among soil–foundation–structure system. Computers & Structures, **80**(20–21): 1579–
644 1594. doi:10.1016/S0045-7949(02)00115-3.

645 Elsaid, A., and Seracino, R. 2014. Rapid assessment of foundation scour using the dynamic
646 features of bridge superstructure. Construction and Building Materials, **50**: 42–49.
647 Elsevier Ltd. doi:10.1016/j.conbuildmat.2013.08.079.

648 De Falco, F., and Mele, R. 2002. The monitoring of bridges for scour by sonar and sedimetri.
649 NDT&E International, **35**: 117–123.

650 Farrar, C.R., Baker, W.E., Bell, T.M., Cone, K.M., Darling, T.W., Duffey, T.A., Eklund, A.,
651 and Migliori, A. 1994. Dynamic characterization and damage detection in the I-40
652 bridge over the Rio Grande.

653 Farrar, C.R.C.R., Duffey, T.A., Cornwell, P.J.P.J., and Doebling, S.W.S.W. 1999. Excitation
654 methods for bridge structures. *In* Proceedings of the 17th International Modal Analysis
655 Conference Kissimmee. Kissimmee, FL. pp. 1063–1068.

656 Fisher, M., Chowdhury, M.N., Khan, A. a., and Atamturktur, S. 2013. An evaluation of scour
657 measurement devices. Flow Measurement and Instrumentation, **33**: 55–67. Elsevier.
658 doi:10.1016/j.flowmeasinst.2013.05.001.

659 Fitzgerald, P.C., Malekjafarian, A., Bhowmik, B., Prendergast, L.J., Cahill, P., Kim, C.,
660 Hazra, B., Pakrashi, V., and Obrien, E.J. 2019a. Scour Damage Detection and Structural
661 Health Monitoring of a Laboratory-Scaled Bridge Using a Vibration Energy Harvesting
662 Device. Sensors, **19**(11).

663 Fitzgerald, P.C., Malekjafarian, A., Cantero, D., OBrien, E.J., and Prendergast, L.J. 2019b.
664 Drive-by scour monitoring of railway bridges using a wavelet-based approach.
665 Engineering Structures, **191**(February): 1–11. Elsevier.

doi:10.1016/j.engstruct.2019.04.046.

Foti, S., and Sabia, D. 2011. Influence of Foundation Scour on the Dynamic Response of an Existing Bridge. Journal Of Bridge Engineering, **16**(2): 295–304. doi:10.1061/(ASCE)BE.1943-5592.0000146.

González, A., and Hester, D. 2013. An investigation into the acceleration response of a damaged beam-type structure to a moving force. Journal of Sound and Vibration, **332**(13): 3201–3217. doi:10.1016/j.jsv.2013.01.024.

Green, F., and Cebon, D. 1997. Dynamic interaction between heavy vehicles and highway bridges. Computers and Structures, **62**(2): 253–264.

Hamill, L. 1999. Bridge Hydraulics. E.& F.N. Spon, London.

Hester, D., and González, A. 2012. A wavelet-based damage detection algorithm based on bridge acceleration response to a vehicle. Mechanical Systems and Signal Processing, **28**: 145–166. doi:10.1016/j.ymssp.2011.06.007.

Hunt, B.E. 2009. NCHRP synthesis 396: Monitoring Scour Critical Bridges - A Synthesis of Highway Practice. *In* Transportation Research Board. Washington, DC.

Kassir, M.K., Bandyopadhyay, K.K., and Reich, M. 1996. Thermal degradation of concrete in the temperature range from ambient to 315 ºC.

Klinga, J. V., and Alipour, A. 2015. Assessment of structural integrity of bridges under extreme scour conditions. Engineering Structures, **82**: 55–71. Elsevier Ltd. doi:10.1016/j.engstruct.2014.07.021.

Kong, X., Ho, S.C.M., Song, G., and Cai, C.S. 2017. Scour Monitoring System Using Fiber Bragg Grating Sensors and Water-Swellable Polymers. Journal of Bridge Engineering, **22**(7): 04017029. doi:10.1061/(ASCE)BE.1943-5592.0001062.

Kullaa, J. 2003. Damage detection of the Z24 bridge using control charts. Mechanical Systems and Signal Processing, **17**(1): 163–170. doi:10.1006/mssp.2002.1555.

Kwon, Y.W., and Bang, H. 2000. The Finite Element Method using MATLAB. CRC Press, Inc., Boca Raton, FL.

Limongelli, M.P. 2010. Frequency response function interpolation for damage detection under changing environment. Mechanical Systems and Signal Processing, **24**(8): 2898–2913. doi:10.1016/j.ymssp.2010.03.004.

Lyons, R. 2011. Understanding digital signal processing. *In* 3rd Editio. Prentice Hall, Boston, MA.

Maddison, B. 2012. Scour failure of bridges. Proceedings of the ICE - Forensic Engineering, **165**(FE1): 39–52.

Malekjafarian, A., and OBrien, E. 2017. On the use of a passing vehicle for the estimation of bridge mode shapes. Journal of Sound and Vibration, **397**: 77–91. Available from http://www.sciencedirect.com/science/article/pii/S0022460X17301979 [accessed 31 May 2017].

Malekjafarian, A., and OBrien, E.J. 2014. Identification of bridge mode shapes using Short Time Frequency Domain Decomposition of the responses measured in a passing vehicle. Engineering Structures, **81**: 386–397. doi:10.1016/j.engstruct.2014.10.007.

Melville, B.W., and Coleman, S.E. 2000. Bridge scour. Water Resources Publications, Highlands Ranch, CO.

O'Brien, E.J., Keogh, D.L., and O'Connor, A.J. 2015. Bridge deck analysis. *In* 2nd Editio. CRC Press.

OBrien, E., and Malekjafarian, A. 2016. A mode shape-based damage detection approach using laser measurement from a vehicle crossing a simply supported bridge. Structural Control and Health Monitoring,. Available from http://onlinelibrary.wiley.com/doi/10.1002/stc.1841/pdf [accessed 31 May 2017].

Prendergast, L.J., and Gavin, K. 2014. A review of bridge scour monitoring techniques. Journal of Rock Mechanics and Geotechnical Engineering, **6**(2): 138–149. doi:10.1016/j.jrmge.2014.01.007.

Prendergast, L.J., Gavin, K., and Hester, D. 2017. Isolating the location of scour-induced stiffness loss in bridges using local modal behaviour. Journal of Civil Structural Health Monitoring, **7**(4): 483–503. Springer Berlin Heidelberg. doi:10.1007/s13349-017-0238-3.

Prendergast, L.J., Hester, D., and Gavin, K. 2016a. Determining the presence of scour around bridge foundations using vehicle-induced vibrations. Journal Of Bridge Engineering, **21**(10). doi:10.1061/(ASCE)BE.1943-5592.0000931.

Prendergast, L.J., Hester, D., and Gavin, K. 2016b. Development of a Vehicle-Bridge-Soil Dynamic Interaction Model for Scour Damage Modelling. Shock and Vibration, **2016**. doi:10.1155/2016/7871089.

Prendergast, L.J., Hester, D., Gavin, K., and O'Sullivan, J.J. 2013. An investigation of the changes in the natural frequency of a pile affected by scour. Journal of Sound and Vibration, **332**(25): 6685–6702. doi:http://dx.doi.org/10.1016/j.jsv.2013.08.020i.

Prendergast, L.J., Reale, C., and Gavin, K. 2018. Probabilistic examination of the change in eigenfrequencies of an offshore wind turbine under progressive scour incorporating soil spatial variability. Marine Structures, **57**: 87–104. doi:10.1016/j.marstruc.2017.09.009.

Shirole, A.M., and Holt, R.C. 1991. Planning for a comprehensive bridge safety assurance program. *In* Transport Research Record. Transport Research Board, Washington, DC. pp. 39–50.

Sohn, H. 2007. Effects of environmental and operational variability on structural health monitoring. Philosophical transactions. Series A, Mathematical, physical, and engineering sciences, **365**(1851): 539–560. doi:10.1098/rsta.2006.1935.

Sohn, H., Farra, C.R., Hemez, F., Shunk, D., Stinemates, D., Nadler, B., and Czarmecki, J. 2004. A Review of Structural Health Monitoring Literature : 1996 – 2001.

Tedesco, J.W., McDougal, W.G., and Allen Ross, C. 1999. Structural Dynamics: Theory and Applications.

Wardhana, K., and Hadipriono, F.C. 2003. Analysis of Recent Bridge Failures in the United States. Journal of Performance of Constructed Facilities, **17**(3): 144–151. doi:10.1061/(ASCE)0887-3828(2003)17:3(144).

Winkler, E. 1867. Theory of elasticity and strength. Dominicus Prague.

Xiong, W., Kong, B., Tang, P., and Ye, J. 2018. Vibration-Based Identification for the

749 Presence of Scouring of Cable-Stayed Bridges. Journal of Aerospace Engineering,
750 **31**(2). doi:10.1061/(ASCE)AS.1943-5525.0000826.

751 Yang, F., and Fonder, G. 1996. An iterative solution method for dynamic response of bridge–
752 vehicles systems. Earthquake engineering & structural dynamics, **25**: 195–215.
753 Available from http://onlinelibrary.wiley.com/doi/10.1002/(SICI)1096-
754 9845(199602)25:2%3C195::AID-EQE547%3E3.0.CO;2-R/abstract [accessed 23 April
755 2014].

756 Yang, Y., Yau, J., and Wu, Y. 2004. Vehicle-bridge interaction dynamics. World Scientific,
757 Singapore. Available from
758 http://www.worldscientific.com/doi/pdf/10.1142/9789812567178_fmatter [accessed 23
759 April 2014].

760 Yu, X. 2009. Time Domain Reflectometry Automatic Bridge Scour Measurement System:
761 Principles and Potentials. Structural Health Monitoring, **8**(6): 463–476.
762 doi:10.1177/1475921709340965.

763 Zarafshan, A., Iranmanesh, A., and Ansari, F. 2012. Vibration-Based Method and Sensor for
764 Monitoring of Bridge Scour. Journal Of Bridge Engineering, **17**(6): 829–838.
765 doi:10.1061/(ASCE)BE.1943-5592.0000362.

766 Žnidarič, A., O'Brien, E.J., Corbally, R., Kreslin, M., Cantero, D., and Kalin, J. 2013.
767 Technical specification for the Class A Bridge WIM system.

768